Dynamics of Photoinduced Electron Transfer in an Amphiphilic A^{2+}-S-D Triad Molecule†

Masaru Sakomura,‡ Su Lin,§ Thomas A. Moore,§ Ana L. Moore,§ Devens Gust,§ and Masamichi Fujihira*,‖

Department of Material Science, Yokohama National University, Tokiwadai, Hodogaya-ku, Yokohama 240-8501, Japan, Department of Chemistry and Biochemistry, Arizona State University, Tempe, Arizona 85287, Department of Biomolecular Engineering, Tokyo Institute of Technology, Nagatsuta, Midori-ku, Yokohama 226-8501, Japan

Received: July 6, 2001; In Final Form: December 3, 2001

An amphiphilic A^{2+}-S-D triad molecule and its reference compounds, S−D, A^{2+}-S, and S type molecules, were synthesized and studied using time-resolved transient absorption spectroscopy. The three moieties in the triad, i.e., an electron acceptor moiety (A^{2+}, viologen), a sensitizer moiety (S, perylene), and an electron donor moiety (D, ferrocene), were linearly combined by sigma-bonded tunneling bridges. Intramolecular electron transfer reactions were initiated by photoexcitation of the S moiety to $^1S^*$, and the long-lived final charge separated state, $A^{\bullet+}$-S-$D^{\bullet+}$, was formed. Although the yield of the initial charge separated state, $A^{\bullet+}$-$S^{\bullet+}$-D, was very high (0.93), the overall yield of the final charge separated state was ca. 0.2. The rate of the backward electron transfer from $A^{\bullet+}$ to $S^{\bullet+}$ was observed to be two times lower than that of the forward electron transfer from $^1S^*$ to A^{2+}, suggesting that with suitable molecular engineering, the yield of long-lived charge separation in such triads could be improved.

1. Introduction

Synthetic molecular photodiodes based on the mimicry of natural photosynthetic reaction centers and consisting of covalently linked chromophores and redox moieties (dyad, triad, tetrad, and others) have been actively studied, and many papers have appeared.[1−19] Such molecules have potential for application to supramolecular systems for artificial photosynthesis and ultrafast optoelectronic molecular devices that perform logic functions.[20−32]

The first organic molecular photocells based on dye sensitization by covalently bound molecules on an oxide semiconductor electrode were reported by some of us in the mid-1970s as an approach to the design of optoelectronic components with molecular dimensions.[33] An improved photovoltaic molecular device with an amphiphilic triad molecule unidirectionally oriented at an electrode surface was reported in 1985.[34] In this amphiphilic triad three moieties, a dicationic electron acceptor (A^{2+}, viologen), a neutral sensitizer (S, pyrene), and a neutral electron donor (D, ferrocene), were combined to give a *folded* triad S-A^{2+}-D in which the active components were linked by sigma-bonded tunneling bridges. At an air−water interface, the triad forms stable mixed monolayers with arachidic acid, in which the dicationic hydrophilic A^{2+} moiety of the triad is oriented toward the water and two hydrophobic alkyl chains terminated by S and D subunits extend into the air.

In such monolayers, an ordered spatial arrangement of the A^{2+}, S, and D moieties across the interface was expected under high surface pressures, owing to the difference in the length of the two alkyl chains (C_6 and C_{11}) linking A^{2+} to S and D, respectively. Later, a modified S-A^{2+}-D triad was synthesized in order to improve the relationship of the two distances.[35] In this highly ordered, *folded* type S-A^{2+}-D triad, two step intramolecular electron transfer was initiated through light absorption by the pyrene sensitizer moiety S to form its first excited singlet state ($^1S^*$). As a result, formation of a long-lived charge separated state S-$A^{\bullet+}$-$D^{\bullet+}$ would be expected, given the energies of the various ions of the oriented triad.[1,20,34,36] A photoelectric conversion device was readily fabricated by transferring the monolayer film containing the folded-type triad onto a gold optically semitransparent electrode (AuOTE) using the Langmuir−Blodgett (LB) technique. Spatial ordering with A^{2+} near the AuOTE surface, followed by S, and finally by D at the external surface of the film was consistent with the observation of anodic photocurrents, whose direction was in accordance with the expected vectorial flow of electrons, in an electrochemical cell with the LB modified AuOTE as a working electrode.[34,35] The AuOTE was intentionally used to show that charge was separated by the oriented triad, and not by a space charge region at a semiconductor surface.[33] However, the photoelectric conversion efficiency was diminished by quenching of $^1S^*$ by gold.

In an attempt to produce a more functional conformation relating the A^{2+}, S, and D moieties and to improve the orientation of the triad molecules in the monolayer, a *linear* type A^{2+}-S-D triad was also synthesized.[37] In this triad, the three moieties are linked sequentially with one another in the order A^{2+}, S, and D. Thus an asymmetric spatial arrangement of the components in monomolecular layer assemblies is expected to exhibit the same order. A mixed monolayer of the *linear* A^{2+}-S-D triad with behenic acid exhibited a much higher photocurrent than that of the *folded* S-A^{2+}-D triad mentioned above. This indicates that an improved spatial arrangement of the A^{2+}, S, and D moieties was indeed attained for the linear triad molecule in the mixed monolayer.

† Part of the special issue "Noboru Mataga Festschrift".

* Corresponding author. E-mail: mfujihir@bio.titech.ac.jp. Fax: +81-45-924-5817.

‡ Department of Material Science.

§ Department of Chemistry and Biochemistry.

‖ Department of Biomolecular Engineering.

10.1021/jp012566v CCC: $22.00
Published on Web 02/14/2002

SCHEME 1

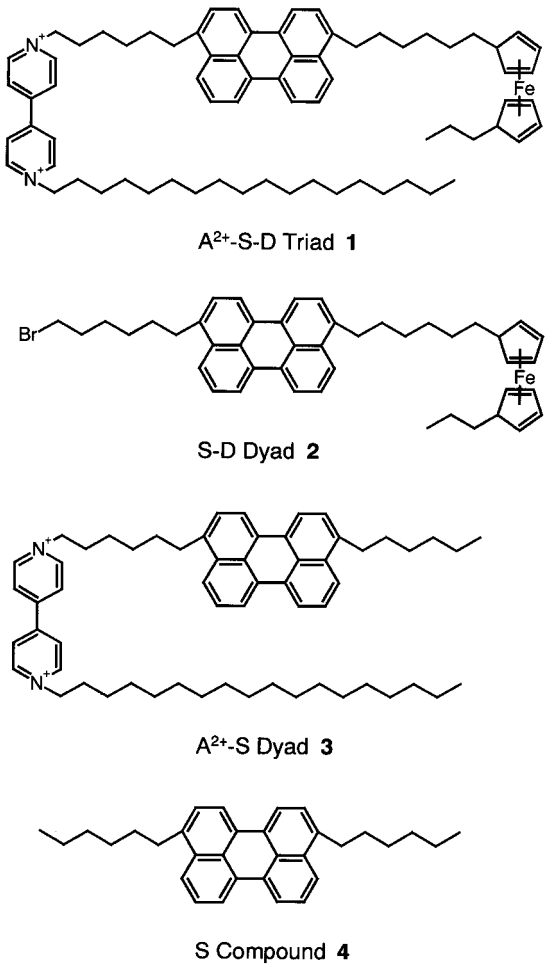

Since amphiphilicity is needed to promote unidirectional molecular orientation in LB assemblies, viologen was used as the acceptor moiety in the variety of triad molecules we have synthesized.[1] For the S moiety, a dialkyl pyrene, an alkyl-acyl pyrene, or an alkyl-acyl perylene have been used, while an alkyl ferrocene, an acyl ferrocene, or a diacyl ferrocene has been adopted for the D moiety. Photoelectric conversion of the LB assemblies consisting of these triads has been substantiated by observing photocurrent and photovoltage using electrochemical cells[34,35,37] and scanning surface potential microscopy (SSPM),[2,22,25] respectively. However, the charge separation and recombination processes within these triad molecules have never been kinetically elucidated in detail, although charge separation in S−D and A^{2+}-S dyads has been investigated by picosecond fluorescence lifetime measurements.[1,20,36,38]

In the present work, syntheses of a new A^{2+}-S-D triad (**1** in Scheme 1) as well as its reference compounds **2**, **3**, and **4** will be described. In the new triad, viologen, dialkyl perylene, and dialkyl ferrocene moieties serve as the A^{2+}, S, and D moieties, respectively. Second, the energetics of photoinduced electron transfer in A^{2+}-S-D triad **1** based on spectroscopic and electrochemical data of each moiety will be presented. Finally, transient absorption measurements which allow elucidation of the dynamics of photoinduced charge separation and recombination in the triad will be reported.

2. Results

Materials. In the course of the syntheses, two substituents were introduced into the perylene rings of compounds **1**−**4** by two successive Friedel−Crafts acylation reactions. For example, compound **4**, which has two hexyl groups in the perylene ring, was synthesized by following procedure.

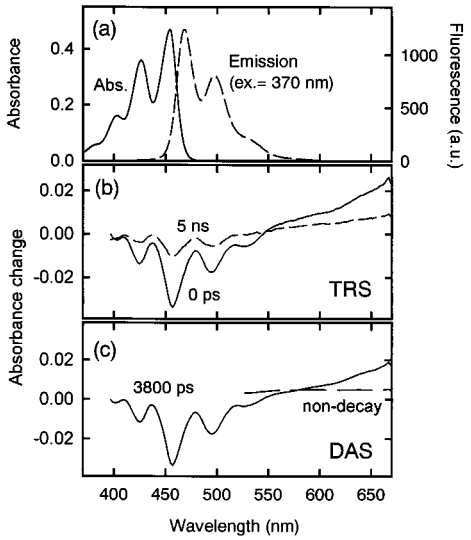

Figure 1. (a) Steady-state spectra of S model compound **4**. The steady state absorption spectrum (solid line) shows three bands at 405, 425, and 455 nm. The fluorescence emission spectrum (dashed line) exhibits essentially a mirror image of the absorption spectrum, peaking at 470, 500, and 535 nm. (b) Time-resolved spectra recorded at 0 ps (solid line) and at 5 ns (dashed line). (c) Decay associated spectra obtained from global analysis of the transient absorption data recorded on the 5 ns time scale.

Friedel−Crafts acylation of perylene with *n*-hexanoyl chloride yielded exclusively 3-hexanoylperylene. After transforming the carbonyl group to a methylene, the resulting 3-hexylperylene was acylated with *n*-hexanoyl chloride in the same manner. The second electrophilic acylation reaction had been expected to occur at the positions of high electron availability, i.e., 4, 9, and 10 in the ring of 3-hexylperylene. However, NMR studies indicated that the product consisted of a mixture of only 3-hexyl-9-hexanoylperylene and 3-hexyl-10-hexanoylperylene. The inhibition of the formation of 3-hexyl-4-hexanoylperylene is attributed to the inability of *n*-hexanoyl chloride to access the 4 position due to the steric hindrance at position 3 in the perylene ring. We proceeded with the synthesis using a mixture of the two regioisomers. Subsequent reduction of the acyl groups of the two regioisomers to alkyl groups provided a mixture of 3,9- and 3,10-dihexylperylene (ca. 4:6). Isolation and purification of isomers was so difficult and wasteful that we have employed the mixture of the two regioisomers in further studies of compound **4**. In addition, use of the mixture was expected to discourage crystallization and thus phase separation in mixed LB monolayers.[39]

Similarly, each of the compounds **1**−**3** was obtained as a mixture of the corresponding two regioisomers. In any of these compounds, the molar ratio of the two regioisomers was also ca. 4:6. Note that only the structural formulas of the slightly dominant products are indicated in Scheme 1 as the compounds **1**−**4**.

Electrochemical Data. A cyclic voltammetric study on the compound **4** (dialkyl perylene) was carried out in acetonitrile solution. The first reduction and oxidation potentials are −2.17 and +0.53 V, respectively, vs the ferrocene/ferrocenium ($Fc/Fc^{\bullet+}$) couple. As shown in Figure 1a, the spectral overlap between the fluorescence and the absorption of **4** was observed at a wavelength of 460 nm (2.70 eV) which corresponds to the 0−0 transition energy. The redox potentials for the excited

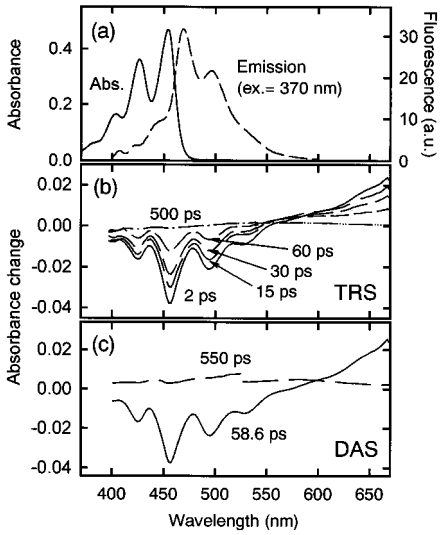

Figure 2. (a) Steady-state absorption spectrum (solid line) and fluorescence emission spectrum (dashed line) of S−D compound **2**. (b) Time-resolved spectra recorded at 2 ps (solid line), 15 ps (dashed line), 30 ps (dashed line), 60 ps (dashed line), and 500 ps (dotted−dashed line). (c) Decay associated spectra obtained from global analysis of the transient absorption data recorded on the 550 ps time scale.

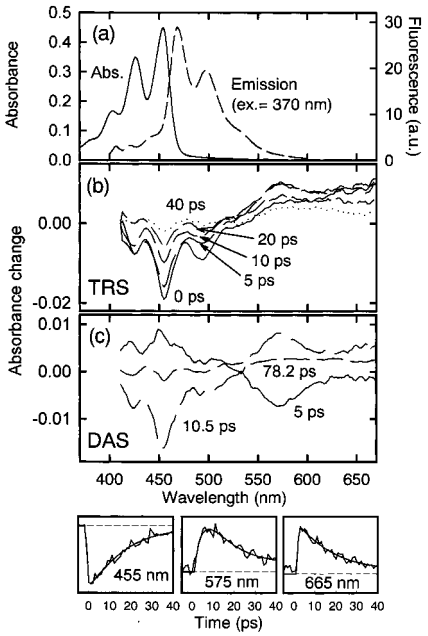

Figure 3. (a) Steady-state absorption spectrum (solid line) and fluorescence emission spectrum (dashed line) of A^{2+}-S compound **3**. (b) Time-resolved spectra recorded at 0 ps (solid line), 5 ps (dashed line), 10 ps (dashed line), 20 ps (dashed line), and 40 ps (dotted line). (c) Decay associated spectra obtained from global analysis of the transient absorption data recorded on the 50 ps time scale. The bottom panels show kinetic traces at selected wavelengths. The smooth lines are the fitting curves. The dashed lines represent zero lines. The vertical scale is arbitrary.

sensitizer moiety were determined from these redox potentials in the ground state and the 0−0 transition energy.[40] On the other hand, the 0−0 transition energy of the donor (dialkyl ferrocene) moiety was estimated to be 530 nm (2.34 eV) only from the longest wavelength of the absorption spectrum of dialkyl ferrocene because the excited donor moiety itself has no fluorescence.

On the bases of the energetics of the electron transfer derived above and the potentials for the ground-state acceptor (viologen) and donor moieties obtained from previous studies,[41−43] possible pathways of deactivation of the photoexcited A^{2+}-^{1}S*-D triad **1** to the final long-lived charge-separated $A^{\bullet+}$-S-$D^{\bullet+}$ state as well as to the ground A^{2+}-S-D state are depicted in Figure 6. Here, a slight difference in oxidation potentials between ferrocene and dialkyl ferrocene is taken into account.[43]

Steady-State Absorption Spectra. The steady-state absorption spectrum of model S compound **4** in benzonitrile solution (Figure 1a) features maxima at 405, 425, and 455 nm. The absorption spectra of S-D, A^{2+}-S, and A^{2+}-S-D, **2**, **3**, and **1**, respectively, in this wavelength region (Figures 2a, 3a, and 4a) are very similar to that of **4**. Thus, the interactions between the aromatic rings of the S and A or D moieties of the dyads or the triad, such as charge transfer complex formation, are not appreciable at the ground states. In the spectra of the S−D dyad and the A^{2+}-S-D triad the absorption of the dialkyl ferrocene moiety, which is expected to appear as a broad band ranging from 360 to 530 nm, is too small to be obvious. However, its spectral overlap with perylene emission suggests the possibility of energy transfer quenching of the excited perylene moiety by the dialkyl ferrocene moiety (step vi in Figure 6).

Fluorescence Spectra. The fluorescence emission spectra of S−D dyad **2**, A^{2+}−S dyad **3**, and A^{2+}-S-D triad **1** in benzonitrile solution with excitation at 370 nm are very similar in shape to that of model S compound **4**, with maxima 470, 500, and 535 nm (Figures 1a, 2a, 3a, and 4a). A small shoulder or a peak around 440 nm in Figures 2a, 3a, and 4a is due to a background emission from the solvent. The fluorescence quantum yields of **1** − **3** are much lower than that of **4**, which indicates that attachment of the viologen and/or ferrocene moiety to the perylene provides the new pathways for the deactivation of the

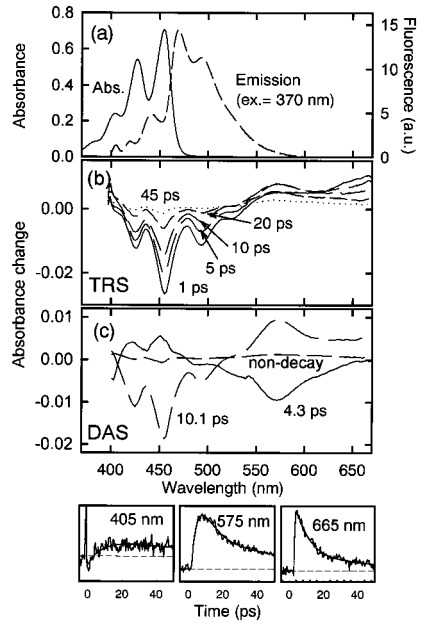

Figure 4. (a) Steady-state absorption spectrum (solid line) and fluorescence emission spectrum (dashed line) of A^{2+}-S-D triad **1**. (b) Time-resolved spectra recorded at 1 ps (solid line), 5 ps (dashed line), 10 ps (dashed line), 20 ps (dashed line), and 45 ps (dotted line). (c) Decay associated spectra obtained from global analysis of the transient absorption data recorded on the 50 ps time scale. The bottom panels show kinetic traces at selected wavelengths. The smooth lines are the fitting curves. The dashed lines represent zero lines. The vertical scale is arbitrary.

perylene first excited singlet state (^{1}S*) as illustrated in Figure 6. The fluorescence quenching of **1**−**3** estimated from transient absorption spectroscopic studies described in the next seems to be slightly more efficient than that estimated from the fluores-

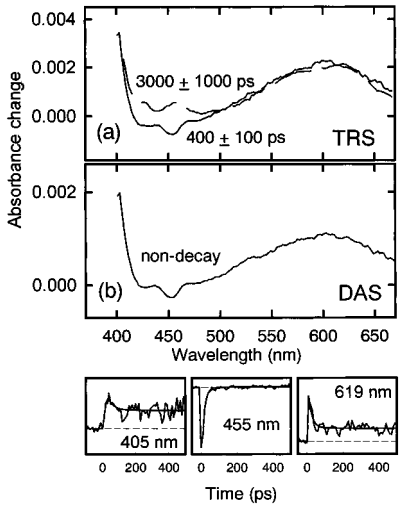

Figure 5. (a) Time-resolved spectra for A^{2+}-S-D triad **1** averaged over 400 ± 100 ps (solid line), and 3000 ± 1000 ps (dashed line). (b) The nondecaying component of the decay associated spectrum obtained from global analysis of the transient absorption data recorded on the 4000 ps time scale. The bottom panels show kinetic traces at selected wavelengths from a measurement over 500 ps. The smooth lines are the fitting curves. The dashed lines represent zero lines. The vertical scale is arbitrary.

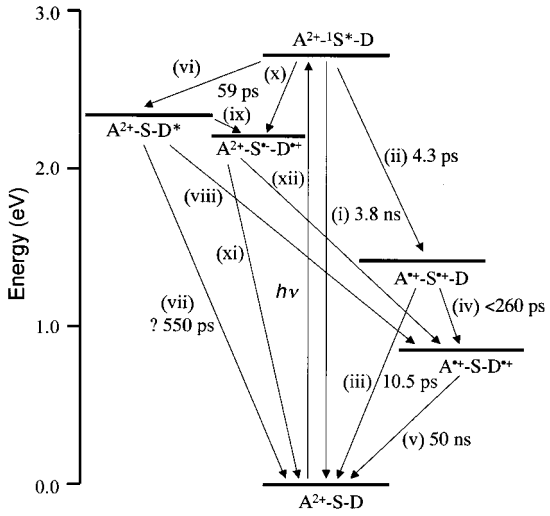

Figure 6. The kinetic scheme for A^{2+}-S-D triad **1** in benzonitrile. The $A^{\bullet+}$-$S^{\bullet+}$-D state is formed in high quantum yield (93%), based on the kinetic results (numbers listed are used in the yield calculation). The final $A^{\bullet+}$-S-$D^{\bullet+}$ state is formed via a pathway through a major initial product, i.e., $A^{\bullet+}$-$S^{\bullet+}$-D (steps ii and iv), as well as via three pathways through minor initial products, i.e., A^{2+}-S-D* and A^{2+}-$S^{\bullet-}$-$D^{\bullet+}$. The latter three pathways are steps vi and viii, steps vi, ix, and xii, and steps x and xii. The quantum yield of $A^{\bullet+}$-S-$D^{\bullet+}$ was caluculated erroneously to be 0.035, based on global analysis of the kinetic data for the pathway through the major initial product (see text). From the curves for absorbance vs time at various wavelengths, at which abosrbance for S* and $S^{\bullet+}$ is negligible in comparison with that for $A^{\bullet+}$, the overall quantum yield of $A^{\bullet+}$-S-$D^{\bullet+}$ was estimated to be ca. 0.2. The final state is relatively long-lived (50 ns).

cence spectra in Figures 2−4. The deviation, however, can be explained by the background emission from the solvent.

Transient Absorption Experiments. To identify and determine kinetic parameters for photophysical processes in compounds **1**−**4**, we undertook transient absorption experiments on the picosecond time scale. Samples were dissolved in benzonitrile, placed in a cuvette with a 2-mm or 5-mm path length, and excited at 400 nm with 100-fs laser pulses.

Figures 1b and 1c show time-resolved spectra (TRS) and decay-associated spectra (DAS) of model S compound **4**, respectively. In the wavelength region from 400 to 550 nm in Figure 1b, there is a net transient absorption decrease, with spectral minima at 425, 460, 500, and 535 nm in the transient absorption spectrum at early times. These bands are due to a mixture of ground-state bleaching and stimulated emission from the first excited singlet state of the perylene moiety (^{1}S*). A broad absorption increase at 550 nm and above is also observed, and is due to the excited-state absorption of ^{1}S*. Global analysis of the transient absorption recorded on the 4.5 ns time scale results in one lifetime of 3.8 ns. This result clearly indicates that there is no significant difference in the lifetimes of the perylene first excited singlet states of the 3,9 and 3,10 regioisomers of **4**. A long-lived, featureless component was also obtained in the fitting of the long wavelength region, it is probably due to a background offset.

One elementary intramolecular electron transfer step in the acceptor-sensitizer-donor system was studied by transient absorption measurements on S−D dyad **2**. Figure 2b shows that at early times the transient absorption spectra of **2** exhibit the characteristics of ^{1}S*, but this state decays much faster than it does in **4**. Global analysis yields two kinetic components. The 58.6 ps component has negative amplitude around 460 nm, whereas the 550 ps component features positive amplitude around 450−650 nm (Figure 2c). Since the decay-associated spectrum of the 550 ps component does not show the ground-state bleaching characteristic of ^{1}S*, it is likely due to the formation of the excited state of the dialkyl ferrocene moiety via energy transfer (step vi in Figure 6) and the succeeding deactivation of the excited state of the donor moiety D* (step vii in Figure 6). Note that the first excited state of ferrocene is not singlet. [44] After the formation of D*, the electron transfer from D* to S is also energetically possible (step ix in Figure 6). However, the absorption change due to the formation of the perylene anion radical[45] was not observed at all. This can be rationalized by a mechanism in which, due to a large energy gap, the backward charge recombination (step xi in Figure 6) must be much faster than that of the forward charge separation process (step ix in Figure 6) with a small energy gap. In the second mechanism, the slow process with a lifetime of 550 ps may correspond to the step ix. Another likely mechanism is slow photoinduced charge separation of ^{1}S*-D to $S^{\bullet-}$-$D^{\bullet+}$ with a lifetime of 58.6 ps (step x in Figure 6) followed by the much faster recombination to the ground-state S−D (step xi in Figure 6). The absence of the absorption spectrum of $S^{\bullet-}$ in Figure 2 was also rationalized by the much faster recombination than the separation, which can be readily expected from the difference in the energy gaps between the charge separation and recombination. In this third mechanism, there is no slow process. Therefore, if it is the case, the observed slow process with a lifetime of 550 ps is ascribable to such a background offset as observed in Figure 1 as the nondecay component. At present, we cannot conclude which is the most probable one among the above three mechanisms for the time-resolved spectral changes in Figure 2.

Another elementary step was studied using A^{2+}-S dyad **3**. Time-resolved spectra of **3** within the first 40 ps (Figure 3b) show that in addition to absorbance changes similar to those observed for **4** in the wavelength region from 400 to 550 nm, there is a positive band around 575 nm. The kinetic trace at 575 nm shows the rise and decay of this absorbance within the first 40 ps after laser excitation. In the DAS, three components are needed to fit the kinetics in entire wavelength region. There

is a 5 ps component showing positive bands at 420 and 450 nm, and a negative band centered at 575 nm. The 575 nm band is ascribed to the formation of the perylene cation-radical[45,46] in the charge separated state $A^{\bullet+}$-$S^{\bullet+}$, and the spectrum in the 410−525 nm region possibly to a further build-up of S due to either $^1S^*$ or $S^{\bullet+}$ in addition to the prompt rise due to direct excitation of S. The accompanying absorption change due to the formation of the viologen cation radical, which should appear as a broad band in the wavelength region from 500 to 700 nm is not obvious because the molar absorption coefficient at an absorption peak (600 nm) within the wide wavelength region of the viologen cation-radical (ca. 1.5×10^4 M^{-1} cm^{-1})[47] is smaller than that of the perylene cation-radical (ca. 4.8×10^4 M^{-1} cm^{-1}).[46] The majority of the $A^{\bullet+}$-$S^{\bullet+}$ state decays to A^{2+}-S with a lifetime of 10.5 ps. The DAS of the third component (lifetime = 78.2 ps) shows a spectral profile similar to that of the 10.5-ps component, but with less than 10% of the amplitude. This is probably due to a second, minor extended conformation of the molecule. The presence of the long-lived conformational state of $A^{\bullet+}$-$S^{\bullet+}$ is ascribable to the flexibility of the spacer alkyl chain and also to the Coulombic repulsion between the positive charges in the charge-separated $A^{\bullet+}$-$S^{\bullet+}$ state.

Now we can interpret the A^{2+}-S-D data based on knowledge obtained from the model compounds. Figures 4 and 5 show time-resolved spectral changes and kinetic traces from 400 to 670 nm for A^{2+}-S-D triad **1** measured on the 50, 500, and 4000 ps time scales. The measurement at early times shows the decay of perylene stimulated emission at 500 nm, and absorption increases below 410 nm and around 575 nm. The absorption increase below 410 nm is due to the formation of the viologen cation radical and that at 575 nm is due to the formation of the perylene cation radical. The formation of the viologen cation radical should also induce an absorbance increase in a wide wavelength region from 500 to 700 nm, which is superimposed on the 575 nm band of the perylene cation radical, as in the A^{2+}-S dyad. At longer time delays (after 100 ps, Figure 5a), the bleaching bands in the 410−500 nm region disappear, representing the complete recovery of the perylene ground-state bleaching (Figure 5, 455 nm trace). The perylene cation radical band at 575 nm also decays completely. In addition to the sharp peak at 400 nm, the broad absorbance band in the long wavelength region centered at 600 nm remained even after 4000 ps. These two bands are ascribed to the viologen cation radical,[47] which has a lifetime on the nanosecond time scale and shows nondecaying kinetics on the time scale measured here (Figure 5, 405 and 619 nm traces).

Global analysis of the A^{2+}-S-D data returns three kinetic components. Their decay-associated spectra are plotted in Figures 4c and 5b. The 4.3-ps components have the same profiles as the 5-ps components in the A^{2+}-S dyad. Here, the formation of $A^{\bullet+}$-$S^{\bullet+}$ radical pair is made more obvious than that in Figure 3c by the appearance of negative bands of a 400 nm sharp peak and a broad band above 500 nm due to $A^{\bullet+}$ in addition to a negative band centered at 575 nm due to $S^{\bullet+}$. Therefore, we suggest that they represent the process of $A^{\bullet+}$-$S^{\bullet+}$-D formation from A^{2+}-$^1S^*$-D. The $A^{\bullet+}$-$S^{\bullet+}$-D state decays with a lifetime of 10.1 ps. This lifetime is very similar to that of $A^{\bullet+}$-$S^{\bullet+}$ in dyad **3**, as if the majority of the $A^{\bullet+}$-$S^{\bullet+}$-D state decayed directly to the ground-state A^{2+}-S-D. However, the long-lived component clearly shows the viologen cation radical formation in fairly reasonable yield. Since the molar absorption coefficients of the ferrocene excited state and cation radical[44,48−53] are very small in the wavelength region measured, their contributions are not obvious in the DAS. We can attribute the long-lived state to $A^{\bullet+}$-S-$D^{\bullet+}$. A kinetic measurement on the nanosecond time scale has shown that the lifetime of this state is ca. 50 ns.[54]

3. Discussion

Model Compounds. The lifetime of $^1S^*$ of model S compound **4**, τ_s, was 3.8 ns in benzonitrile solution (step i in Figure 6). Attaching the viologen moiety, as in dyad **3**, drastically reduces the lifetime of $^1S^*$ by introducing a new decay pathway, photoinduced electron transfer to the attached viologen moiety, to yield $A^{\bullet+}$-$S^{\bullet+}$ (step ii in Figure 6). The rate constant for photoinduced electron transfer, k_{cs}, is estimated from the transient absorption results to be 2.0×10^{11} s^{-1} and the quantum yield of $A^{\bullet+}$-$S^{\bullet+}$ ($k_{cs}/(k_{cs} + 1/\tau_s)$) equals 1.00. The $A^{\bullet+}$-$S^{\bullet+}$ state recombines to the ground state with a lifetime of 10.5 ps ($k_{cr} = 9.5 \times 10^{10}$ s^{-1}). The fact that the intramolecular charge separation process in the A^{2+}-S dyad system is two times more rapid than the corresponding charge recombination process (step iii in Figure 6) is desirable for achieving subsequent charge separation by attaching an additional redox component in a triad. The results for S-D dyad **2** suggest that (i) the perylene first excited singlet state of $^1S^*$-D decays by the energy transfer and succeeding deactivation of the excited energy acceptor (steps vi and vii in Figure 6), (ii) the energy transfer followed by succeeding charge separation and recomination (steps vi, ix, and xi in Figure 6), or (iii) the photoinduced electron transfer followed by the recombination (steps x and xi in Figure 6), as described already. For the first and second mechanisms, a fast process with a rate constant of 1.7×10^{10} s^{-1} is ascribable solely to the energy transfer step, while a slower process with a rate constant of 1.8×10^9 s^{-1} can be ascribed to the steps vii and ix, respectively. In the third mechanism, only the fast process with a rate constant of 1.7×10^{10} s^{-1} should be observable.

Triad 1. Turning now to **1**, the kinetic behavior in benzonitrile may be discussed with pathways illustrated in Figure 6. The energies of the excited states have been estimated from spectroscopic data, and the energies of the charge-separated states are based on the cyclic voltammetric results presented above and obtained from the literature.[41−43] No corrections for Coulombic effects have been made.

In the absence of the viologen acceptor and ferrocene donor, the lifetime of the perylene first excited singlet state is 3.8 ns, as determined from studies of model S compound **4**. Thus, k_1, the rate constant for step i in Figure 6, may be estimated as 2.6×10^8 s^{-1}. Global analysis of the transient absorption data for A^{2+}-S-D triad **1** in the 400−670 nm region demonstrated that the absorption of the perylene cation-radical rises with a time constant of 4.3 ps. Thus the rate constant for step ii, k_2, is estimated to be 2.3×10^{11} s^{-1}. If we estimate k_6 (or k_{10}) as 1.7×10^{10} s^{-1}, as was found for S-D dyad **2**, the quantum yield of $A^{\bullet+}$-$S^{\bullet+}$-D, Φ_2, is 0.93. In other words, the quantum yield of the initial product in the left pathways in Figure 6, i.e., A^{2+}-S-D* and/or A^{2+}-$S^{\bullet-}$-$D^{\bullet+}$, Φ_6 and/or Φ_{10} is 0.07.

The intermediate $A^{\bullet+}$-$S^{\bullet+}$-D state decays by two routes: charge recombination to the ground state (step iii) and electron transfer from the ferrocene moiety to give the final $A^{\bullet+}$-S-$D^{\bullet+}$ species (step iv). Global analysis shows that $A^{\bullet+}$-$S^{\bullet+}$-D decays with a time constant $\tau_c = 10.1$ ps. The rate constant for step iv, k_4, is given by eq 1:

$$k_4 = (1/\tau_c) - k_3 \qquad (1)$$

If we estimate k_3 as 9.5×10^{10} s^{-1}, as was found for A^{2+}-S dyad **3**, then $k_4 = 3.8 \times 10^9$ s^{-1}. The overall quantum yield of

$A^{\bullet+}$-S-$D^{\bullet+}$, $\Phi_{A^{\bullet+}\text{-S-}D^{\bullet+}}$, given by eq 2 is 0.035.

$$\Phi_{A^{\bullet+}\text{-S-}D^{\bullet+}} = \Phi_2(k_4/(k_3 + k_4)) \quad (2)$$

However, we have to be more careful in the argument above. When we did global analysis on the time-resolved spectral changes in Figure 3 for A^{2+}-S dyad **3**, we fitted the data with a function in the following form.[55]

$$A(t,\lambda) = \mathrm{DAS}_1\exp(-t/\tau_1) + \mathrm{DAS}_2\exp(-t/\tau_2) + \mathrm{DAS}_3\exp(-t/\tau_3) \quad (3)$$

where τ_1 is 5 ps, τ_2 is 10.5 ps, and τ_3 is 78.2 ps. For A^{2+}-S dyad **3**, the global analysis described above gave correct kinetic parameters, because the decay process of A^{2+}-^{1}S* is simply described as a successive reaction scheme as follows:

$$A^{2+}\text{-}{}^1S^* \xrightarrow[\text{fast}]{} A^{\bullet+}\text{-}S^{\bullet+} \xrightarrow[\text{slow}]{} A^{2+}\text{-S} \quad (4)$$

In the second slow charge recombination process, the decay rate of $S^{\bullet+}$ is the same as that for $A^{\bullet+}$. In addtion, these decay rates were also the same as the rates for reproduction of A^{2+} and S. The same is true for the first fast photoinduced electron transfer process.

However, in the second steps for A^{2+}-^{1}S*-D, the decay profile of the $S^{\bullet+}$ in $A^{\bullet+}$-$S^{\bullet+}$-D is not the same as the decay profile of $A^{\bullet+}$, because part of $A^{\bullet+}$ is converted into A^{2+} in the form of A^{2+}-S-D, but the remainder of $A^{\bullet+}$ becomes long-lived $A^{\bullet+}$ in the form of $A^{\bullet+}$-S-$D^{\bullet+}$. In addition, the absorption of $A^{\bullet+}$ in the wavelengths between 400 and 650 nm is not negligible in comparison with that of $S^{\bullet+}$. For this reason, global analysis by eq 3 is, in principle, not strictly applicable to determination of the decay rate of $A^{\bullet+}$-$S^{\bullet+}$-D. The fitted estimate for τ_2, namely 10.1 ps, could in fact be longer than the true decay rate of $A^{\bullet+}$-$S^{\bullet+}$-D, because of the contribution from the absorbance in the wavelengths between 400 and 650 nm due to the long-lived $A^{\bullet+}$.

In this way, 0.035 for the overall quantum yield of $A^{\bullet+}$-S-$D^{\bullet+}$, $\Phi_{A^{\bullet+}\text{-S-}D^{\bullet+}}$, given by eq 2 could be lower than the true value. In addition a long-lived extended conformation of $A^{\bullet+}$-$S^{\bullet+}$-D similar to that attributed to the long-lived decay component of $A^{\bullet+}$-$S^{\bullet+}$ with a lifetime of 78.2 ps may produce $A^{\bullet+}$-S-$D^{\bullet+}$ in a much higher yield, although the amount of the extended conformation may be less than 10% that of the short-lived conformer. In addition to the above pathway, the left pathways in Figure 6 via steps vi and viii, steps vi, ix, and xii, and steps x and xii, may also contribute to the formation of the final charge-separated state, $A^{\bullet+}$-S-$D^{\bullet+}$, although the yield by these pathways should be less than 0.07 (i.e., the quantum yield of the intermediate products in the left pathways in Figure 6, described above).

For an alternative estimate of $\Phi_{A^{\bullet+}\text{-S-}D^{\bullet+}}$, we examined the rise and decay of the absorbances at wavelengths in which the observed absorbances were mainly attributed to the formation and the disappearance of $A^{\bullet+}$. For example, the peak absorbance for $A^{\bullet+}$ is about three times larger than the final value (nondecay $A^{\bullet+}$) from the curve for absorbance vs time at 619 nm in Figure 5. At this wavelength, absorbance for S* and $S^{\bullet+}$ is negligible in comparison with absorbance for $A^{\bullet+}$. In other words, this curve can be regarded as the change in concentration of $A^{\bullet+}$ as a function of time in the first approximation. From this curve for $A^{\bullet+}$, we have to conclude that the overall quantum yield of $A^{\bullet+}$-S-$D^{\bullet+}$, $\Phi_{A^{\bullet+}\text{-S-}D^{\bullet+}}$ can be at least 0.2. The kinetics in Figure 5 were, however, measured with a low time resolution (10 ps/step) and thus the peak value near time zero might not be the true maximum. We finally tried to estimate the yield by combining the data sets with 0.5 and 10 ps resolution at various wavelengths and obtained the yield of ca. 0.2. According to the results of the nanosecond transient absorption studies,[54] the final $A^{\bullet+}$-S-$D^{\bullet+}$ state decays to the ground state with $k_5 = 2.0 \times 10^7\ s^{-1}$.

As discussed above, the final charge separated state is mostly produced by the following pathway:

$$A^{2+}\text{-}{}^1S^*\text{-D} \xrightarrow[\text{fast}]{} A^{\bullet+}\text{-}S^{\bullet+}\text{-D} \xrightarrow[\text{slow}]{} A^{\bullet+}\text{-S-}D^{\bullet+} \quad (5)$$

with a faster branching reaction of the intermediate state, $A^{\bullet+}$-$S^{\bullet+}$-D, directly to the ground state, A^{2+}-S-D (see Figure 6). In each step, two cationic moieties resulted within the A^{2+}-S-D triad molecule by the intramolecular electron transfer processes after the photoexcitation of the S moiety. In the course of the electron transfer processes, the Coulombic repulsive force between the two cations would be expected to stretch the molecular conformations, which contributes to inhibit the recombinations of separated charges. Thus it would be important for the molecular design of the triad that step ii is faster than step x. As shown by the studies about the dependence of exciplex formations on the length of methylene bridges of dyad molecules,[56] the molecular conformations of the triad can be affected by the bridge lengths. In particular, the rate constants of initial steps ii and x forming $A^{\bullet+}$-$S^{\bullet+}$-D and A^{2+}-$S^{\bullet-}$-$D^{\bullet+}$, respectively, may strongly depend on the bridge lengths. The dependence of the bridge lengths will be studied soon.

4. Conclusions

The time-resolved absorption studies revealed that a two-step electron transfer sequence in triad **1** generated the $A^{\bullet+}$-S-$D^{\bullet+}$ state. However, the overall yield for this state was found to be relatively low (ca. 0.2), even though the $A^{\bullet+}$-$S^{\bullet+}$-D initial charge-separated state was produced with very high quantum yield (0.93). The rate constant of the back electron transfer from $A^{\bullet+}$-$S^{\bullet+}$-D was observed to be two times lower than that of the corresponding forward electron transfer. This result suggests that a higher overall yield should be possible if a larger rate constant for electron transfer from D to $S^{\bullet+}$ could be attained. We are now studying new triads in which the sigma-bonded tunneling bridge between the D and S moieties is shorter than a 6 carbon alkyl chain in order to achieve this goal. With regard to the studies of electron transfer in optoelectronic applications discussed above, it should be noted that the kinetics of intramolecular electron transfer processes in the A^{2+}-S-D triad and A^{2+}-S and S−D dyads in benzonitrile solutions obtained in this study might not correspond to those in a monolayer or a micellar system.

5. Experimental Section

Synthesis. A^{2+}-S-D triad **1**, model S−D dyad **2**, model A^{2+}-S dyad **3**, and model S compound **4** were prepared as described below. More detailed synthetic procedures for compounds **1** − **4** and for intermediates 1-(3-perylenyl)-6-bromohexane, 3-hexylperylene, 6-(1-(1′-propanoyl)ferrocenyl)-6-oxohexanoic acid, and *N*-octadecyl-4,4′-bipyridinium tosylate will be completely described elsewhere.

The dyad **2** was prepared as a precursor of the triad **1**. It should be noted that the S−D dyad **2** was isolated as a mixture of regioisomeric 3,9- and 3,10-disubstituted perylene-ferrocene dyads (3,9-S−D and 3,10-S−D) in the molar ratio ca. 4:6. The molar ratio was determined by 270 MHz ^{1}H NMR and MOPAC PM3 calculations. Thus the triad **1** produced from a mixture of

3,9- and 3,10-S-D is a mixture of the corresponding two regioisomers 3,9- and 3,10-A^{2+}-S-D, respectively. Similarly, dyad **3** and compound **4** were produced as mixtures of regioisomeric 3,9- and 3,10-A^{2+}-S and 3,9- and 3,10-S in almost the same molar ratio ca. 4:6. Only the structural formulas of the major products are shown in Scheme 1 as **1**−**4**.

*S-D Dyad **2***.To a mixture of 6-(1-(1′-propanoyl)ferrocenyl)-6-oxohexanoic acid (1.2 g, 3.25 mmol) and benzene (12 mL) predried with sodium was added phosphorus pentachloride (0.7 g, 3.4 mmol). The mixture was stirred at room temperature under nitrogen for 30 min and then at 50 °C for 20 min. After the mixture was cooled to room temperature, dichloromethane (100 mL) and 1-(3-perylenyl)-6-bromohexane (1.35 g, 3.25 mmol) were added. After the 1-(3-perylenyl)-6-bromohexane was completely dissolved, aluminum chloride (1.6 g, 0.012 mol) was added to the mixture at 0 °C. The mixture was stirred at 0−10 °C for 30 min under nitrogen. The resulting purple solution was poured onto 200 g of crushed ice and the mixture was extracted with 100 mL of dichloromethane. The dichloromethane solution was dried over anhydrous magnesium sulfate. Removal of dichloromethane on a rotary evaporator left a red oily residue. The crude product was purified by column chromatography on silica gel with a mixture of toluene and acetone (50:1) as an eluant to yield 1.04 g (42%) of the acylated perylene derivative, Br-$(CH_2)_6$-Pe-$CO(CH_2)_4CO$−Fc-COC_2H_5, where -Pe- and -Fc- represent a perylene and a ferrocene group, respectively.

The three carbonyl groups on the perylene and ferrocene rings in the product were converted to methylenes by the following procedures. To a mixture of the acylated compound (0.8 g, 1.04 mmol) and dry dichloromethane (20 mL) under an atmosphere of nitrogen was added dropwise a solution of titanium(IV) chloride[57] (0.4 mL, 3.3 mmol) in dry dichloromethane (10 mL). Triethylsilane (2.2 mL, 14 mmol) was then added to the reaction mixture, and the contents were further stirred at room temperature for 2 days. The reaction mixture was then quenched with aqueous sodium carbonate (15 mL, 5% w/v), and the resulting inorganic precipitate was filtered. The organic layer was separated and dried over anhydrous magnesium sulfate, and the solvent was removed. The oily residue was purified by column chromatography on silica gel, eluting with chloroform to yield 71% (535 mg): ^{1}H NMR (270 MHz, $CDCl_3$) δ 0.91 (3H, t, J = 7.3 Hz, $-CH_3$), 1.42−1.53 (12H, m, $-CH_2$), 1.71 (4H, m, $PeCH_2-CH_2$), 1.81 (2H, m, $BrCH_2-CH_2$), 2.27 (4H, m, Fc-CH_2), 2.94 (4H, m, Pe-CH_2), 3.36 (2H, t, J = 6.9 Hz, Br−CH_2), 3.94 (8H, s, Fc-H), 7.22−7.27 (2H, m, Pe(3,9-S−D) 2,8-H, Pe(3,10-S−D) 2,11-H), 7.42−7.47 (2H, m, Pe(3,9-S−D) 5,11-H, Pe(3,10-S−D) 5,8-H), 7.75−7.83 (2H, m, Pe(3,9-S−D) 4,10-H, Pe(3,10-S−D) 4,9-H), 8.00−8.06 (2H, m, Pe(3,9-S−D) 1,7-H, Pe(3,10-S−D) 1,12-H), 8.10−8.16 (2H, m, Pe(3,9-S−D) 6,12-H, Pe(3,10-S−D) 6,7-H).

A^{2+}-S-D *Triad **1***. A mixture of S−D dyad **2** (230 mg, 0.32 mmol), *N*-octadecyl-4,4′-bipyridinium tosylate (370 mg, 0.64 mmol), and dry acetonitrile (15 mL) was stirred at 80−85 °C for 2 days under a nitrogen atmosphere. A crude precipitate was filtered off, washed with hot acetone several times and recrystallized two times from ethanol to yield 22% (92 mg): ^{1}H NMR (270 MHz, DMSO-d_6, 60 °C) δ 0.85 (6H, t, J = 7.26 Hz, $-CH_3$), 1.24−1.47 (42H, m, $-CH_2$), 1.71 (4H, m, $PeCH_2-CH_2$), 1.98 (4H, m, $N^+CH_2-CH_2$), 2.21−2.30 (9.1H (as the result of anion exchange, the ratio of counteranions seems to be Br^-:TsO^- = 15:85), m, Fc-CH_2, $^-OSO_2$-ϕ-CH_3), 3.00 (4H, m, Pe-CH_2), 3.93 (8H, d, J = 1.6 Hz, Fc-H), 4.65−4.73 (4H, m, N^+-CH_2), 7.08 (3.4H, d, J = 7.91 Hz, arom(anion)), 7.39 (2H, d, J = 7.58 Hz, Pe(3,9-A^{2+}-S-D) 2,8-H, Pe(3,10-A^{2+}-S-D) 2,11-H), 7.49 (3.4H, d, J = 7.92 Hz, arom(anion)), 7.53−7.59 (2H, m, Pe(3,9-A^{2+}-S-D) 5,11-H, Pe(3,10-A^{2+}-S-D) 5,8-H), 7.90−7.93 (2H, m, Pe(3,9-A^{2+}-S-D) 4,10-H, Pe(3,10-A^{2+}-S-D) 4,9-H), 8.19−8.26 (2H, m, Pe(3,9-A^{2+}-S-D) 1,7-H, Pe(3,10-A^{2+}-S-D) 1,12-H), 8.29−8.35 (2H, m, Pe(3,9-A^{2+}-S-D) 6,12-H, Pe(3,10-A^{2+}-S-D) 6,7-H), 8.72 (2H, d, J = 6.6 Hz, arom(bipyridine)), 9.33 (2H, m, arom(bipyridine)).

A^{2+}-*S Dyad **3***. A dichloromethane solution (20 mL) containing *n*-hexanoyl chloride (320 mg, 2.38 mmol) was added dropwise to a mixture of 1-(3-perylenyl)-6-bromohexane (1.0 g, 2.41 mmol), aluminum chloride (700 mg, 5.24 mmol), and dry dichloromethane (300 mL) over a period of 30 min at 0 °C. The reaction mixture was stirred for 1 h and then poured onto 500 g of crushed ice. The lower, dichloromethane layer was separated and washed with water several times and dried over anhydrous magnesium sulfate. The solvent was distilled at reduced pressure and the crude product was chromatographed on silica gel with toluene to give Br-$(CH_2)_6$-Pe-$CO(CH_2)_4CH_3$ (840 mg, 1.64 mmol). Reduction of the carbonyl group was carried out by mixing the acylated perylene derivative (520 mg, 1.00 mmol), trifluoroacetic acid (1.60 g, 14.0 mmol), triethylsilane (280 mg, 2.4 mmol), and dichloromethane (5 mL) and stirring this mixture overnight. Dichloromethane, excess trifluoroacetic acid, and silyl derivatives were removed by vacuum distillation. The residue was purified by column chromatography on silica gel with toluene to yield 210 mg (0.42 mmol) of the reduced compound, Br-$(CH_2)_6$-Pe-$(CH_2)_5CH_3$. A mixture of the reduced compound (150 mg, 0.30 mmol), *N*-octadecyl-4,4′-bipyridinium tosylate (260 mg, 0.45 mmol), and dry acetonitrile (10 mL) was stirred at 80−85 °C for 2 days under a nitrogen atmosphere. A crude precipitate was filtered off, washed with hot acetone several times and recrystallized two times from ethanol to give 110 mg (0.10 mmol) of dyad **3** (9.4% total yield based on 1-(3-perylenyl)-6-bromohexane): ^{1}H NMR (270 MHz, DMSO-d_6, 60 °C) δ 0.83−0.90 (6H, m, $-CH_3$), 1.24−1.45 (40H, m, $-CH_2$), 1.68−1.73 (4H, m, $PeCH_2-CH_2$), 1.99 (4H, m, $N^+CH_2-CH_2$), 2.28 (3H, s, $^-OSO_2$-ϕ-CH_3), 2.97−3.00 (4H, m, Pe-CH_2), 4.68−4.71 (4H, m, N^+-CH_2), 7.08 (2H, d, J = 8.24 Hz, arom(anion)), 7.39 (2H, d, J = 7.91 Hz, Pe(3,9-A^{2+}-S) 2,8-H, Pe(3,10-A^{2+}-S) 2,11-H), 7.49 (2H, d, J = 8.26 Hz, arom(anion)), 7.54−7.60 (2H, m, Pe(3,9-A^{2+}-S) 5,11-H, Pe-(3,10-A^{2+}-S) 5,8-H), 7.91−7.93 (2H, m, Pe(3,9-A^{2+}-S) 4,10-H, Pe(3,10-A^{2+}-S) 4,9-H), 8.20−8.22 (2H, m, Pe(3,9-A^{2+}-S) 1,7-H, Pe(3,10-A^{2+}-S) 1,12-H), 8.33−8.36 (2H, m, Pe(3,9-A^{2+}-S) 6,12-H, Pe(3,10-A^{2+}-S) 6,7-H), 8.73 (2H, d, J = 6.3 Hz, arom(bipyridine)), 9.33 (2H, m, arom(bipyridine)).

*Model S Compound **4**.* A dichloromethane solution (20 mL) containing *n*-hexanoyl chloride (360 mg, 2.68 mmol) was added dropwise to a mixture of 3-hexylperylene (1.0 g, 2.98 mmol), aluminum chloride (900 mg, 6.74 mmol), and dry dichloromethane (300 mL) over about 30 min at 0 °C. The reaction mixture was stirred for 1 h and then poured onto 500 g of crushed ice. The lower dichloromethane layer was separated and washed with water several times and dried over anhydrous magnesium sulfate. The solvent was distilled at reduced pressure and the crude product was chromatographed on silica gel with toluene to give $CH_3(CH_2)_6$−Pe-$CO(CH_2)_4CH_3$ (800 mg, 1.84 mmol). Reduction of carbonyl group was carried out by mixing the acylated perylene derivative (500 mg, 1.15 mmol), trifluoroacetic acid (1.84 g, 16.1 mmol), triethylsilane (320 mg, 2.76 mmol), and dichloromethane (5 mL) and stirring this mixture overnight. Dichloromethane, excess trifluoroacetic acid, and silyl derivatives were removed by vacuum distillation. The residue was purified with column chromatography on silica gel with

toluene to give 200 mg (0.48 mmol) model S compound **4** (43% total yield based on 3-hexylperylene): ^{1}H NMR (270 MHz, $CDCl_3$) δ 0.90 (6H, t, $J = 6.8$ Hz, $-CH_3$), 1.32−1.46 (12H, m, $-CH_2$), 1.70−1.81 (4H, m, $PeCH_2$-CH_2), 3.00 (4H, t, $J = 7.8$ Hz, Pe-CH_2), 7.31 (2H, d, $J = 7.6$ Hz, Pe(3,9-S) 2,8-H, Pe(3,-10-S) 2,11-H), 7.49 (2H, t, $J = 8.1$ Hz, Pe(3,9-S) 5,11-H, Pe-(3,10-S) 5,8-H), 7.83−7.88 (2H, m, Pe(3,9-S) 4,10-H, Pe(3,10-S) 4,9-H), 8.06−8.12 (2H, m, Pe(3,9-S) 1,7-H, Pe(3,10-S) 1,12-H), 8.15−8.21 (2H, m, Pe(3,9-S) 6,12-H, Pe(3,10-S) 6,7-H).

Instrumental Techniques. ^{1}H NMR spectra were recorded with tetramethylsilane as an internal standard at 270 MHz. Preparative column chromatography was carried out on silica gel 60 (Merck, size: 63−200 μm). Ultraviolet−visible spectra were measured on a Shimadzu UV-265FW UV−Vis spectrometer, and fluorescence spectra were measured on a JASCO FP-777 using optically dilute samples and corrected for instrument response. Cyclic voltammetric measurements were carried out with an ALS Model 600A electrochemical analyzer. The electrochemical measurements were performed in acetonitrile at ambient temperature with a glassy carbon working electrode, a Ag/Ag^+ reference electrode, and a platinum wire counter electrode. The electrolyte was 0.1 M tetra-*n*-butylammonium perchorate, and ferrocene was employed as an internal reference redox system.

The femtosecond transient absorption spectrometer consists of a pulsed laser source and a pump−probe optical setup. The laser pulse train was provided by a Ti:Sapphire regenerative amplifier (Clark-MXR, Model CPA-1000) pumped by a diode-pumped CW solid-state laser (Spectra Physics, Model Millennia V). The typical laser pulse was 100 fs at 800 nm, with a pulse energy of 0.9 mJ at a repetition rate of 1 kHz. Most of the laser energy (80%) was frequency doubled to generate the second harmonic at 400 nm. The 400 nm beam was sent through a computer-controlled delay line and used as the excitation pulse. The rest of the laser output (20%) was focused into a 1.2 cm rotating quartz plate to generate a white light continuum. The continuum beam was further split into two identical parts, which were used as the probe and reference beams. The polarization of the excitation beam was set at the magic angle (54.7°) with respect to the probe and reference beams. The probe and reference signals were focused into two separated optical fiber bundles coupled to a spectrograph (Acton Research SP-275). The spectra were acquired on a dual diode array detector (Princeton Instruments DPDA-1024). The sample was contained in an optical cell with a 2- or 5-mm path length. The sample was stirred to prevent laser heating. A typical absorbance of 0.5−1 at the excitation wavelength was used. The global analysis and decay-associated spectra (DAS) were developed after deconvolution of the observed kinetics with the excitation pulse and correction for the spectral dispersion of the probe beam.

Acknowledgment. This work was in part supported by a Grant-in-Aid for Scientific Research (A) (06403020, 11355036) to M.F. from the Ministry of Education, Science, Sports, and Culture and also supported in part by a grant to M.F. and M.S. under the Japan-U.S.A. Cooperative Photoconversion and Photosynthesis Research Program from the Ministry of Education, Science, Sports, and Culture. This work was supported in part by a grant to D.G., T.A.M., and A.L.M. from the U. S. Department of Energy (DE-FG03-93ER14404).

References and Notes

(1) Fujihira, M. *Thin Films* **1995**, *20*, 239−277.
(2) Sakomura, M.; Oono, T.; Fujihira, M. *Thin Solid Films* **1998**, *327−329*, 708−711.
(3) Gust, D.; Moore, T. A. *Adv. Photochem.* **1991**, *16*, 1−65.
(4) Gust, D.; Moore, T. A.; Moore, A. L. *Acc. Chem. Res.* **1993**, *26*, 198−205.
(5) Bahr, J. L.; Kuciauskas, D.; Liddell, P.; Moore, A.; Moore, T. A.; Gust, D. *Photochem. Photobiol.* **2000**, *72*, 528−611.
(6) Kuciauskas, D.; Liddell, P. A.; Lin, S.; Stone, S. G.; Moore, A. L.; Moore, T. A.; Gust, D. J. *Phys. Chem. B* **2000**, *104*, 4307−4321.
(7) Kuciauskas, D.; Liddell, P. A.; Lin, S.; Johnson, T. E.; Weghorn, S. J.; Lindsey, J. S.; Moore, A. L.; Moore, T. A.; Gust, D. *J. Am. Chem. Soc.* **1999**, *121*, 8604−8614.
(8) Liddell, P. A.; Sumida, J. P.; Macpherson, A. N.; Noss, L.; Seely, G. R.; Clark, K. N.; Moore, A. L.; Moore, T. A.; Gust, D. *Photochem. Photobiol.* **1994**, *60*, 537−541.
(9) Liddell, P. A.; Kuciauskas, D.; Sumida, J. P.; Nash, B.; Nguyen, D.; Moore, A. L.; Moore, T. A.; Gust, D. *J. Am. Chem. Soc.* **1997**, *119*, 1400−1405.
(10) Wasielewski, M. R. *Chem. Rev.* **1992**, *92*, 435−461.
(11) Bixon, M.; Fajer, J.; Feher, G.; Freed, J. H.; Gamliel, D.; Hoff, A. J.; Levanon, H.; Mobius, K.; Nechushtai, R.; Norrris, J. R.; Scherz, A.; Sessler, J. L.; Stehlik, D. *Isr. J. Chem.* **1992**, *32*, 449−455.
(12) Osuka, A.; Noya, G.; Taniguchi, S.; Okada, T.; Nishimura, Y.; Yamazaki, I.; Mataga, N. *Chem. Eur. J.* **2000**, *6*, 33−46.
(13) Asahi, T.; Ohkohchi, M.; Matsusaka, R.; Mataga, N.; Zhang, R. P.; Osuka, A.; Maruyama, K. *J. Am. Chem. Soc.* **1993**, *115*, 5665−5674.
(14) Imahori, H.; Tamaki, K.; Guldi, D. M.; Luo, C.; Fujitsuka, M.; Ito, O.; Sakata, Y.; Fukuzumi, S. *J. Am. Chem. Soc.* **2001**, *123*, 2607−2617.
(15) Imahori, H.; Norieda, H.; Yamada, H.; Nishimura, Y.; Yamazaki, I.; Sakata, Y.; Fukuzumi, S. *J. Am. Chem. Soc.* **2001**, *123*, 100−110.
(16) Imahori, H.; Ozawa, S.; Ushida, K.; Takahashi, M.; Azuma, T.; Ajavakom, A.; Akiyama, T.; Hasegawa, M.; Taniguchi, S.; Okada, T.; Sakata, Y. B*ull. Chem. Soc. Jpn.* **1999**, *72*, 485−502.
(17) Komamine, S.; Fujitsuka, M.; Ito, O.; Moriwaki, K.; Miyata, T.; Ohno, T. *J. Phys. Chem. A* **2000**, *104*, 11497−11504.
(18) Jolliffe, K. A.; Langford, S. J.; Ranasinghe, M. G.; Shephard, M. J.; Paddon-Row, M. N. *J. Org. Chem.* **1999**, *64*, 1238−1246.
(19) Head, N. J.; Thomas, J.; Shephard, M. J.; Paddon-Row: M. N.; Bell, T. D. M.; Cabral, N. M.; Ghiggino, K. P. *J. Photochem. Photobiol.* **2000**, *133*, 105−114.
(20) Fujihira, M. *Adv. Chem. Ser.* **1994**, *240*, 373−394.
(21) Fujihira, M. *NATO ASI Series, Series E: Applied Sciences* **1995**, *286*, 567−591.
(22) Fujihira, M.; Sakomura, M.; Aoki, D.; Koike, A. *Thin Solid Films* **1996**, *273*, 168−176.
(23) Fujihira, M. In *New Developments in Construction and Functions of Organic Thin Films*; Kajiyama, T., Aizawa, M., Eds.; Elsevier Science B. V.: New York, 1996; pp 181−209.
(24) Fujihira, M. *Ann. New York Acad. Sci.* **1998**, *852*, 306−329.
(25) Fujihira, M. *Annu. Rev. Mater. Sci.* **1999**, *29*, 353−380.
(26) O'Neil, M. P.; Niemczyk, M. P.; Svec, W. A.; Gosztola, D.; Gaines, G. L., III; Wasielewski, M. R. *Science* **1992**, *257*, 63−65.
(27) Lukas, A. S.; Bushard, P. J.; Wasielewski, M. R. *J. Am. Chem. Soc.* **2001**, *123*, 2440−2441.
(28) Hayes, R. T.; Wasielewski, M. R.; Gosztola, D. *J. Am. Chem. Soc.* **2000**, *122*, 5563−5567.
(29) Kuciauskas, D.; Liddell, P. A.; Moore, A. L.; Moore, T. A.; Gust, D. *J. Am. Chem. Soc.* **1998**, *120*, 10880−10886.
(30) Gust, D.; Moore, T. A.; Moore, A. L. *Acc. Chem. Res.* **2001**, *34*, 40−48.
(31) Gust, D.; Moore, T. A.; Moore, A. L. *IEEE Eng. Med. Biol.* **1994**, *13*, 58−66.
(32) Debreczeny, M. P.; Svec, W. A.; Wasielewski, M. R. *Science* **1996**, *274*, 584−587.
(33) Osa, T.; Fujihira, M. *Nature* **1976**, *264*, 349−350; Fujihira, M.; Ohishi, N.; Osa, T. *Nature* **1977**, *268*, 226−228.
(34) Fujihira, M.; Nishiyama, K.; Yamada, H. *Thin Solid Films* **1985**, *132*, 77−82.
(35) Fujihira, M.; Yamada, H. *Thin Solid Films* **1988**, *160*, 125−132.
(36) Fujihira, M.; Nishiyama, K.; Aoki, K. *Thin Solid Films* **1988**, *160*, 317−325.
(37) Fujihira, M.; Sakomura, M. *Thin Solid Films* **1989**, *179*, 471−476.
(38) Suga, K.; Fujita, S.; Yamada, H.; Fujihira, M. *Bull. Chem. Soc. Jpn.* **1990**, *63*, 3369−3375.
(39) Fujihira, M.; Kamei, T.; Sakomura, M.; Tatsu, Y.; Kato, Y. *Thin Solid Films* **1989**, *179*, 485−492.
(40) Kalyanasundaram, K. *Coord. Chem. Rev.* **1982**, *46*, 159−244.
(41) Mann, C. K.; Barnes, K. K. *Electrochemical Reactions in Nonaqueous Systems*; Marcel Dekker: New York, 1970.
(42) Hayano, S.; Fujihira, M. *Bull. Chem. Soc. Jpn.* **1971**, *44*, 2051−2055.

(43) Kondo, T.; Yamada, H.; Nishiyama, K.; Suga, K.; Fujihira, M. *Thin Solid Films* **1989**, *179*, 463−469.

(44) Geoffroy, G. L.; Wrighton, M. S. *Organometallic Photochemistry*; Academic Press: New York, 1979.

(45) Shida, T. *Electronic Absorption Spectra of Radical Ions*; Physical Sciences Data 34; Elsevier: Amsterdam, 1988.

(46) Kalintsev, A. G.; Volosov, V. D.; Andreev, R. B. *Opt. Spectrosc.* **1973**, *35*, 96−98.

(47) Watanabe, T.; Honda, K. *J. Phys. Chem.* **1982**, *86*, 2617−2619.

(48) Yang, E. S.; Chan, M.-S.; Wahl, A. C. *J. Phys. Chem.* **1975**, *79*, 2049−2052.

(49) Sohn, Y. S.; Hendrickson, D. N.; Gray, H. B. *J. Am. Chem. Soc.* **1970**, *92*, 3233−3234.

(50) Sohn, Y. S.; Hendrickson, D. N.; Gray, H. B. *J. Am. Chem. Soc.* **1971**, *93*, 3603−3612.

(51) Traverso, O.; Scandola, F. *Inorg. Chim. Acta* **1970**, *4*, 493−498.

(52) Fujihira, Y.; Kuwana, T.; Hartzell, C. R. *Biochem. Biophys. Res. Commun.* **1974**, *61*, 488−493.

(53) Yeh, P.; Kuwana, T. *J. Electrochem. Soc.* **1976**, *123*, 1334−1339.

(54) Sawada, R.; Hirukawa, K.; Sakomura, M.; Fujihira, M. In press.

(55) Holzwarth, A. R. In *Biophysical Techniques in Photosynthesis*; Amesz, J., Hoff, A. J., Eds.; Kluwer Academic Publishers: Norwell, MA, 1996; pp 75−92.

(56) Siemiarczuk, A.; McIntosh, A. R.; Ho, T.-F.; Stillman, M. J.; Roach, K. J.; Weedon, A. C.; Bolton, J. R.; Connolly, J. S. *J. Am. Chem. Soc.* **1983**, *105*, 7224−7230.

(57) Bhattacharyya, S. *J. Org. Chem.* **1998**, *63*, 7101−7102.